Inorganic Chemistry

Article

pubs.acs.org/IC

High-Throughput ab Initio Screening for Two-Dimensional Electride Materials

Tomofumi Tada,*[,†] Seiji Takemoto,[†] Satoru Matsuishi,[†] and Hideo Hosono[†,‡,§,¶]

[†]Materials Research Center for Element Strategy, [‡]Materials and Structures Laboratory, and [§]Frontier Research Center, Tokyo Institute of Technology, 4259 Nagatsuta-cho, Midori-ku, Yokohama, Kanagawa 226-8503, Japan

[¶]ACCEL Project, Japan Science and Technology Agency, 4-1-8 Honcho, Kawaguchi-shi, Saitama 332-0012, Japan

Supporting Information

ABSTRACT: High-throughput ab initio screening of approximately 34000 materials in the Materials Project was conducted to identify two-dimensional (2D) electride materials, which are composed of cationic layers and anionic electrons confined in a 2D empty space. The screening was based on three indicators: (1) a positive total formal charge per formula unit; (2) layered structures for two-dimensionality; (3) empty spaces between the layer units. Three nitrides, Ca_2N, Sr_2N, and Ba_2N, and the carbide Y_2C were identified as 2D electrides, where Ca_2N is the only experimentally confirmed 2D electride (Lee, K.; et al. *Nature* **2013**, *494*, 336−341). Electron density analysis using ionic radii revealed a smaller number of anionic electrons in Y_2C than those in the three nitrides as a result of the partial occupation of the anionic electrons in the d orbitals of Y. In addition, no candidates were identified from the p-block elements, and thus the ab initio screening indicates that the s-block elements (i.e., alkali or alkaline-earth metals) are highly preferable as cation elements. To go beyond the database screening, a tailored modeling was conducted to determine unexplored compounds including the s-block elements that are suitable for 2D electrides. The tailored modeling found that (1) K_2Cl, K_2Br, Rb_2Cl, and Rb_2Br dialkali halides are highly plausible candidates, (2) Li_2F and Na_2Cl dialkali halides are highly challenging candidates, and (3) the $Cs_2O_{1-x}F_x$ halogen-doped dialkali oxide is a promising candidate.

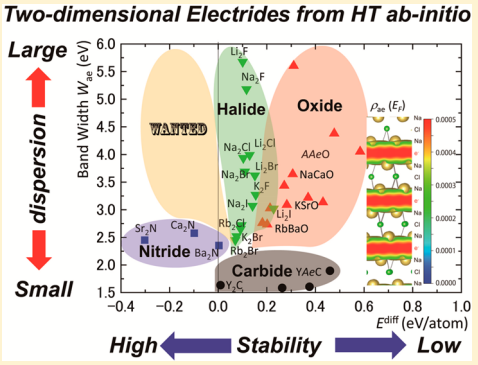

I. INTRODUCTION

Electrides are unique materials in which electrons confined in an empty space behave as anions. The first electride material was synthesized in 1983 by Ellaboudy, Dye, and Smith in which synthesized organic electrides were prepared by dissolving an alkali metal in a solution of crown ether.[1] Although electrides have attracted attention as a novel concept material, the progress of material research on electrides has been slow because of their extreme sensitivity to heat and ambient atmosphere. It was a long-standing issue in this field to realize an electride that was stable at room temperature (RT). The first RT-stable electride was realized in 2003 by the use of an inorganic compound, $12CaO{\cdot}7Al_2O_3$ (C12A7),[2] containing subnanometer-sized cages. These cages are formed from Ca, Al, and O ions and serve as empty spaces for the anionic electrons. When the cages in C12A7 are partially occupied by electrons, the resulting C12A7:e^- is expected to exhibit high electronic conductivity due to electron tunneling through the thin cage walls of the connected cages. In addition, the high electron-donating power, chemical inertness, and strong tolerance to H_2 poisoning of C12A7:e^- enables the synthesis of ammonia by a novel reaction path facilitated by nanosized Ru metal particles.[3]

Although the zero-dimensional (0D) C12A7:e^- electride has a wide range of applications, a two-dimensional (2D) electride is also an attractive material in terms of electroactive applications because 2D materials frequently exhibit unique electronic properties such as superconductivity.[4,5] In 2013, the first 2D electride material, Ca_2N, was identified.[6] Ca_2N has a layered structure composed of cation (Ca) and anion layers (N), and empty spaces develop two dimensionally that are confined between the Ca_2N layers (Figure 1). The formal valence of Ca/N is 2+/3−; therefore, an electron must be added to maintain the charge neutrality; i.e., $[Ca_2N]^{+\bullet}$ e^- is obtained, where e^- denotes the anionic electron. The anionic electron in Ca_2N is loosely confined in the 2D empty space and thus behaves as a 2D electron gas, which was confirmed by electron-transport measurements and the large band dispersion in density functional theory (DFT) calculations.[6] At present, Ca_2N is the only experimentally confirmed 2D electride inorganic material, and the discovery of other 2D electrides is urgently required. However, the synthesis of new materials requires much time; therefore, a systematic screening based on theoretical calculations prior to synthesis is highly preferable.

High-throughput ab initio electronic structure calculations[7,8] are a powerful tool for the systematic screening of new materials using an appropriate materials database. The AFLOW[9] and the Materials Project[10] platforms are the two

Received: June 14, 2014
Published: September 11, 2014

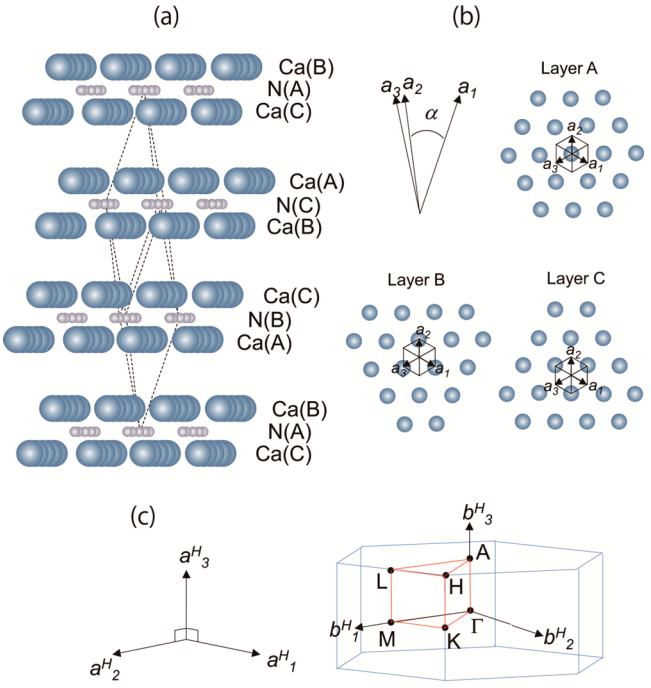

Figure 1. Crystal structure of a Ca_2N 2D electride. (a) Layered structure composed of Ca_2N units. Large/small atoms correspond to Ca/N atoms. Indices A, B, and C in parentheses indicate the layer type shown in part b. (b) Primitive lattice vectors a_1, a_2, and a_3 in the trigonal lattice and the atomic arrangement in layers A, B, and C. (c) Lattice vectors in the hexagonal lattice and the reciprocal vectors together with the high symmetry points (e.g., Γ, K, M, etc.). The vectors a^H_3 and b^H_3 are pointed in the [111] direction of the trigonal lattice. The symmetry points are used for band structure calculations.

pioneering systems in high-throughput ab initio screening for materials exploration. AFLOW has been employed for the exploration of bimetallic systems with thermodynamic stability,[11] and the Materials Project has already succeeded in the prediction of Li-ion batteries.[12] In this study, high-throughput ab initio screening was conducted using the Materials Project database[13,14] for the prediction of 2D electrides. In addition, a tailored modeling, which was designed along the results of the high-throughput screening, was conducted to determine unexplored compounds that are suitable for 2D electrides.

II. METHOD

In materials exploration that employs high-throughput ab initio calculations, indicators (i.e., key physical/chemical quantities for the desired properties) must first be defined or assumed. For example, in a high-throughput ab initio study for photovoltaic cells, the band gap, photon absorptivity, and recombination loss are good indicators.[15] Once the indicators are defined, the candidate materials are almost automatically obtained through high-throughput ab initio calculations from a large database. As a next step, the reliability of the indicators must be confirmed. This requires experimental confirmation that a material (material A) does exhibit the desired properties to verify the candidate materials obtained from high-throughput ab initio screening. If material A is not included in the calculated candidates, then the set of indicators are consequently found to be inappropriate and a new set of indicators must be constructed. High-throughput ab initio screening for 2D electrides was conducted using this strategy.

In previous experimental work on Ca_2N, the indicators for 2D electrides are defined explicitly: (1) positive total formal charge per formula unit, which leads to the addition of anionic electrons to maintain total charge neutrality; (2) layered structures for two-dimensionality; (3) empty spaces between the ionic units for confinement of the anionic electrons. Thus, these three conditions were used as indicators for ab initio screening with the Materials Project ab initio platform.

The Materials Project database of approximately 34000 materials was used for ab initio screening. Automatic screening with the three indicators was not available; however, screening using the crystal systems (e.g., triclinic, cubic, etc.) is possible. Automatic screening was thus conducted under the conditions that (1) the crystal system has trigonal symmetry, because Ca_2N is a trigonal crystal, (2) the number of elements in the unit cell is two (A_nB_m), and (3) the number of sites in the unit cell is less than 15. After the automatic screening, a final screening using the three critical indicators (i.e., formal charge, layered structure, and sufficient 2D space) was performed manually and the ab initio calculations were executed for the remaining candidates.

Ab initio electronic structure calculations based on DFT were performed using the Vienna Ab initio Simulation Package[16] with the projector augmented-wave method[17] and the generalized gradient approximation, as implemented by Perdew, Burke, and Ernzerhoff.[18] The default parameters for energy cutoff, *k*-point mesh, and threshold of energy convergence defined in the Materials Project were adopted.[19] As the final step, the partial electron density was examined to confirm whether the electrons at the Fermi level are confined in the 2D empty spaces between the ionic layers. The VESTA visualization package[20] was used for this purpose. In addition, the number ratio of anionic electrons was introduced to explicitly characterize the 2D electrides.

III. RESULTS AND DISCUSSION

III-1. Ab Initio Screening with the Materials Project. The first screening of the Materials Project with respect to the crystal system and number of elements reduced the approximately 34000 materials to 322. After automatic screening, screening with the three critical indicators was performed for the 322 materials, from which seven materials (Ca_2N, Sr_2N, Ba_2N, Y_2C, Tb_2C, Dy_2C, and Ho_2C) were

Table 1. Relaxed Lattice Data, Calculated Properties for Anionic Electrons, and Energetic Stabilities for Binary Nitrides and Carbides Screened Using the Materials Project[a]

A_2B	ID	VA	VB	FC	a (Å)	α (deg)	a_{ele} (%)	W_{ae} (eV)	v_{2Dmax} ($\times10^8$ cm/s)	v_{zmax} ($\times10^8$ cm/s)	E^{diff} (eV/atom)	C^{ref}
Ca_2N	2686	2+	3−	1+	6.74	31.0	77.1	2.57	0.52 (ΓM)		−0.099	Ca_3N_2, Ca(s)
Sr_2N	1245	2+	3−	1+	7.33	30.5	77.5	2.45	0.44 (ΓM)		−0.302	SrN_2, Sr(s)
Ba_2N	1892	2+	3−	1+	7.96	29.6	72.0	2.35	0.24 (KΓ)		+0.003	Ba_3N, Ba(s)
Y_2C	1334	3+	4−	2+	6.47	32.4	27.4	1.63	0.34 (MK)		+0.009	Y_4C_5, Y(s)

[a]ID denotes the ID number defined in the database. VA, VB, and FC are the formal valences of elements A and B and the total formal charge of the formula unit A_2B, respectively. a and α are the lattice constant and lattice angle, respectively. a_{ele}, W_{ae}, and v_{2Dmax} are the number ratio of anionic electrons at the Fermi level, the bandwidth of anionic electrons, and the 2D-directed maximum velocity of anionic electrons, respectively. The indices in parentheses indicate the corresponding lines between the special *k* points. v_{zmax} is the velocity of electrons on the direction perpendicular to the 2D plane when an energy band crosses the ΓA, LM, or KH lines. E^{diff} is the energy difference with respect to the existing stable compounds (C^{ref}).

dx.doi.org/10.1021/ic501362b | *Inorg. Chem.* 2014, 53, 10347−10358

obtained as candidates for 2D electrides. It should be noted that we also conducted automatic screening based on the restriction of hexagonal or cubic crystal systems; however, no candidates were found; this point will be discussed in a later section. The final candidates for 2D electrides from the Materials Project database were thus restricted to the seven materials found with trigonal symmetry. Table 1 lists the structural data for the three nitrides and Y_2C. The space group of these compounds is $R\bar{3}m$. The Ca_2N 2D electride is included in the list, in addition to other nitrides with the same chemistry (i.e., Sr_2N and Ba_2N), and thus the screening process adopted in this study is considered to be acceptable. Ab initio electronic structure calculations were conducted for the seven materials, and the calculated band structures, partial electron density at the Fermi level, and projected density of states (DOS; not shown) were investigated to determine which materials could be 2D electrides. However, the electronic structure calculations for the f-electron-correlated materials[21] (i.e., Tb_2C, Dy_2C, and Ho_2C) in the seven candidates must be handled carefully by using beyond DFT calculations; this is not suitable for the high-throughput screening based on standard DFT calculations. Therefore, we have excluded the three f-electron systems in this study.

III-1a. Nitride 2D Electrides. The screened binary nitrides are Ca_2N, Sr_2N, and Ba_2N. The screening results are reasonable in terms of the periodicity of elements. The electronic structures of Sr_2N and Ba_2N were already investigated theoretically[22] after experimental examination of Ca_2N was reported in 2013. The calculated band structure and partial electron density around the Fermi level of Ca_2N, Sr_2N, and Ba_2N are shown in Figure 2. The band line of ΓMKΓ runs along the 2D Brillouin zone (Figure 1), and thus the high band dispersion along the line indicates the development of electron distribution on the 2D plane. On the other hand, the band lines of ΓA, LM, and KH are directed perpendicularly to the 2D plane (i.e., [111] direction in the trigonal lattice), and thus no bands cross the Fermi level along the [111]-directed lines, which also indicates the confinement of electrons at the Fermi level onto the 2D spaces. The partial electron density ρ at the Fermi level shows that electrons around the Fermi level are mainly distributed in the empty 2D spaces between the ionic layers; that is, the band crossing the Fermi level originates from the 2D anionic electrons. The band dispersions around the Fermi level in the three nitrides are almost similar, although Ba_2N shows a dispersion slightly different from those of Ca_2N and Sr_2N. The bandwidths (bold lines in Figure 2) of the 2D anionic electrons W_{ae} in Ca_2N, Sr_2N, and Ba_2N are respectively 2.57, 2.45, and 2.35 eV. The Fermi velocities of anionic electrons along the band line of ΓMKΓ can be calculated from the band dispersions, and the maximum velocities of electrons at the Fermi level (v_{2Dmax}) in Ca_2N, Sr_2N, and Ba_2N are determined to be 0.52×10^8, 0.44×10^8, and 0.24×10^8 cm/s on the ΓM, ΓM, and KΓ lines, respectively.

To characterize the 2D anionic electrons more explicitly, the number ratio of 2D anionic electrons at the Fermi level is defined using the partial electron density ρ at $\rho(\mathbf{r},\varepsilon)$ with energy ε and position $\mathbf{r}$ as

$$a_{ele}\,(\%) = \frac{\iiint_{V_{emp}} d\mathbf{r} \int_{E_F-\Delta E}^{E_F+\Delta E} d\varepsilon \rho(\mathbf{r}, \varepsilon)}{\iiint_{V} d\mathbf{r} \int_{E_F-\Delta E}^{E_F+\Delta E} d\varepsilon \rho(\mathbf{r}, \varepsilon)} \times 100 \quad (1)$$

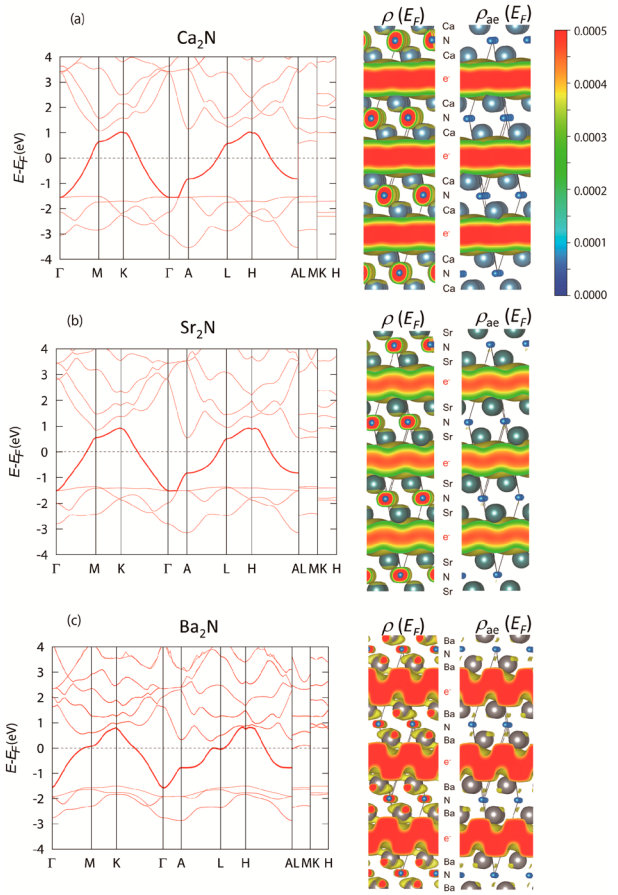

Figure 2. Calculated band structures and partial electron densities for (a) Ca_2N, (b) Sr_2N, and (c) Ba_2N. The red bold lines in the band structures correspond to the energy bands of the anionic electrons confined in 2D empty spaces sandwiched between ionic units. $\rho(E_F)$ is the partial electron density integrated in the energy region from E_F= −0.05 to +0.05 eV, and $\rho_{ae}(E_F)$ is that for the anionic electrons, which are depicted using the color scale (1/bohr^3).

where V is the volume of the unit cell and V_{emp} is the unit cell volume excluding the ionic spheres. The denominator of the equation thus gives the number of electrons in the energy region around the Fermi level with an energy width of $2\Delta E$, and the numerator gives the number of electrons in the empty spaces (i.e., the anionic electrons) in the same energy region. The number ratios a_{ele}, calculated using ΔE of 0.05 eV and the Pauling ionic radii[23] for Ca_2N, Sr_2N, and Ba_2N, are 77.1, 77.5, and 72.0%, respectively. The number ratios of the anionic electrons for Ca_2N and Sr_2N are very high and almost the same, whereas that for Ba_2N is slightly smaller. a_{ele} is qualitatively related to the band dispersion (band shape) and maximum velocity in that the band dispersion and maximum velocity of Ba_2N are different to some extent from those of Ca_2N and Sr_2N. Thus, a_{ele} can be a quantitative indication of the features of 2D electride materials. We also calculated a_{ele} by using the Shannon ionic radii[24,25] and confirmed that the same conclusions are obtained in both approaches (the ionic radii and calculated a_{ele} in both approaches are shown in the Supporting Information). Figure 2 also shows the partial electron density for anionic electrons ρ_{ae}, at the Fermi level, which can be obtained by removing the partial electron density in the ionic spheres from ρ. In the original ρ, small amounts of electrons are distributed around the N atoms in the three

dx.doi.org/10.1021/ic501362b | Inorg. Chem. 2014, 53, 10347−10358

nitrides, but the electrons around the N atom are completely removed in ρ_{ae}. In contrast, the electrons distributed in the 2D empty spaces are almost identical between ρ and ρ_{ae}, which indicates that these electrons in the 2D empty spaces are positioned at the outside of the ionic spheres; i.e., they are anionic electrons. The ratio of the space integrated ρ_{ae} with respect to ρ gives the number ratio of anionic electrons, a_{ele}.

The stability of compounds is also an important factor in the modeling of materials. In particular, the energy difference with respect to the existing materials is a good guide to planning an actual synthesis. Considering Ca_2N, the other stable material is Ca_3N_2 and the energy difference from Ca_3N_2 in an extremely dilute gas condition (i.e., $E^{diff} = E(Ca_2N) - [{}^1/_2E(Ca_3N_2) + {}^1/_2E(Ca(s))]$) is calculated to be −0.099 eV/atom. The total energies of Ca_3N_2 and Ca(s) from the Materials Project database were adopted to make a fair comparison. The negative value of the energy difference indicates the possibility of synthesizing Ca_2N from Ca_3N_2, which is in agreement with the experimental evidence. On the other hand, another definition of E^{diff} can be obtained by using the chemical potentials of gas molecules as $E^{diff} = E(Ca_2N) - [{}^2/_3E(Ca_3N_2) - {}^1/_6E(N_2(g))]$. In this case, the energy difference becomes positive (+0.197 eV/atom), indicating difficulty in synthesizing Ca_2N from a simple mixture of Ca_3N_2 and N_2 gas molecules. In addition, Ca_2N is highly sensitive to oxygen and water molecules in the atmosphere. The stability depending on the gas conditions has to be thus carefully investigated in each target compound, and such specific treatments in each system are not suitable in high-throughput screenings. We therefore adopted the former definition of E^{diff} in this study, assuming an extremely dilute gas condition. Table 1 also lists the calculated number ratios a_{ele}, bandwidths, maximum velocities, and energy differences from the stable compounds in each case. From this data, we can conclude that the two nitrides Sr_2N and Ba_2N are highly promising candidates for 2D electrides, next to Ca_2N.

III-1b. Carbide 2D Electrides and Other Candidates. The screened carbides are Y_2C, Tb_2C, Dy_2C, and Ho_2C, although we focus only on Y_2C in this study. Figure 3 shows the calculated band structure and partial electron density for Y_2C at the Fermi level. The electron distribution is distinctly different from those of Ca_2N, Sr_2N, and Ba_2N. a_{ele} for Y_2C is 27.4%, which indicates that anionic electrons are not the majority of electrons at the Fermi level. Considering the projected DOS (not shown), the major contribution comes from the d orbitals of Y. The different electronic distribution of Y_2C from those of Ca_2N, Sr_2N, and Ba_2N is due to the difference of the element group (i.e., Ca, Sr, and Ba are alkaline-earth metals, whereas Y is a 4d metal). In addition, the formula charge of Y_2C is represented as $[Y_2C]^{2+}\cdot 2e^-$, and the two anionic electrons result in an increase in the Fermi level. Therefore, the decrease in the amount of anionic electrons in Y_2C may lead to a decrease of the Fermi level compared with that expected from the chemical formula, and, in turn, properties similar to those of Ca_2N, Sr_2N, and Ba_2N may appear. This point will be discussed in the later section on anion doping. Although a_{ele} for Y_2C is smaller than those for the three nitrides, this result does not discount the possibility of a Y_2C 2D electride because a single anionic electron can appear per four units of Y_2C.

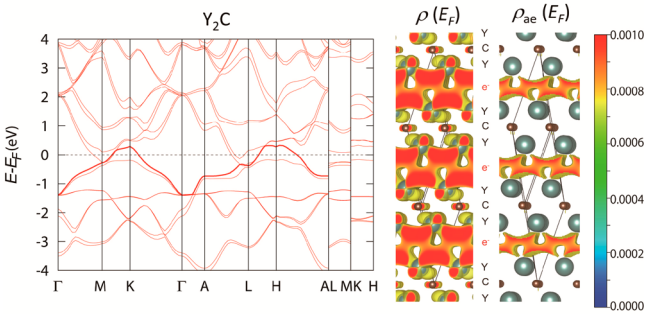

Figure 3. Calculated band structure and partial electron density for Y_2C. The red bold line in the band structure corresponds to the energy band for the anionic electrons, although the amount of anionic electrons in the band is relatively small. $\rho(E_F)$ is the partial electron density integrated in the energy region from E_F= −0.05 to +0.05 eV, and $\rho_{ae}(E_F)$ is that for the anionic electrons, which are depicted using the color scale (1/bohr^3).

As a chemical analogy of Y_2C, Sc_2C is expected to be a 2D electride candidate, although the space group of Sc_2C ($P\bar{3}m1$) is different from that of the seven candidates ($R\bar{3}m$). The electrons at the Fermi level of Sc_2C are localized around the center of Sc ions and empty nanospaces (i.e., interstitial sites), and a_{ele} is calculated to be 16.3%. Therefore, this compound should be investigated further as a different type of electride candidate such as the 0D electride, C12A7:e$^-$. In the same category, Ag_2F with the same space group of $P\bar{3}m1$ was identified. The calculated a_{ele} for Ag_2F is 38.3%, whereas with Sc_2C, the electrons at the Fermi level are weakly localized around the center of Ag ions and interstitial sites.

Three other compounds were identified, Te_2Pt, Te_2Rh, and SiH, in which the 2D empty spaces are included but the assignment of the formal charges is ambiguous compared to the nitrides and carbides. Therefore, these compounds are also possible 2D electride candidates. However, it was confirmed that these materials cannot be 2D electrides because the partial electron densities at the Fermi level are not confined within the 2D empty spaces between ionic layers. Thus, a_{ele} values for Te_2Pt, Te_2Rh, and SiH are very low with calculated values of 4.7, 0.6, and 7.1%, respectively.

III-1c. New Set of Indicators for 2D Electrides. According to the ab initio screening for binary 2D electrides, it can be concluded that the presence of energetically available p and d orbitals in cation layers is not so favorable for electron confinement within the empty spaces between cation layers. Thus, cation layers composed of s-group elements (i.e., alkali or alkaline-earth metals) are highly preferable for 2D electrides. The concept is reasonable because s-group elements show smaller ionization energies than those of p- and d-group elements. In addition, the advantage of s-group elements is also confirmed in a high-pressure electride (HPE);[26] the energy levels of s orbitals become more unstable than those of p orbitals under high-pressure conditions, and electron transfer from s orbitals to an empty space can be expected to occur. We thus systematically extended the exploration to ternary electrides $A_nB_mC_k$, which include alkali or alkaline-earth metals as element A. Like in binary compounds, the trigonal symmetry is again required for the screening. The validity of the symmetry restriction is as follows. The closed packing structure of cations is probably preferable to release electrons into an empty space, and such a closed packing structure is found on the (111) plane in the trigonal symmetry (see Figure 1). Along this strategy, the hexagonal symmetry also might be another acceptable condition, but the presence of the 6-fold rotation axis results in the stacking pattern as $(AB)_n$, showing a clear contrast to $(ABC)_n$ stacking in the 3-fold rotational systems, that is, the

dx.doi.org/10.1021/ic501362b | Inorg. Chem. 2014, 53, 10347−10358

Table 2. Relaxed Lattice Data, Calculated Properties for Anionic Electrons, and Energetic Stabilities for the Dialkali Halides (A_2X) Identified by Screening-Driven Tailored Modeling[a]

A_2B	ID	VA	VB	FC	a (Å)	α (deg)	a_{ele} (%)	W_{ae} (eV)	v_{2Dmax} ($\times 10^8$ cm/s)	v_{zmax} ($\times 10^8$ cm/s)	E^{diff} (eV/atom)	C^{ref}
Li_2F		1+	1−	1+	5.32	31.4	88.4	5.67	0.92 (KΓ)		+0.101	LiF, Li(s)
Li_2Cl		1+	1−	1+	6.18	32.6	85.9	3.99	0.83 (KΓ)		+0.129	LiCl, Li(s)
Li_2Br		1+	1−	1+	6.39	33.5	83.3	3.62	0.79 (KΓ)		+0.151	LiBr, Li(s)
Li_2I		1+	1−	1+	6.77	34.4	76.9	3.02	0.71 (KΓ)		+0.228	LiI, Li(s)
Na_2F		1+	1−	1+	6.22	31.9	88.6	5.18	0.95 (KΓ)		+0.116	NaF, Na(s)
Na_2Cl		1+	1−	1+	7.05	32.6	87.5	3.94	0.83 (KΓ)		+0.103	NaCl, Na(s)
Na_2Br		1+	1−	1+	7.34	32.5	86.5	3.69	0.81 (KΓ)		+0.110	NaBr, Na(s)
Na_2I		1+	1−	1+	7.93	32.4	85.8	3.07	0.75 (KΓ)		+0.141	NaI, Na(s)
K_2F		1+	1−	1+	7.45	31.5	87.2	3.27	0.70 (KΓ)		+0.154	KF, K(s)
K_2Cl		1+	1−	1+	8.21	32.2	88.2	2.72	0.85 (KΓ)		+0.095	KCl, K(s)
K_2Br		1+	1−	1+	8.46	32.0	88.0	2.65	0.65 (KΓ)		+0.092	KBr, K(s)
K_2I		1+	1−	1+	8.97	31.9	87.9	2.43	0.66 (KΓ)	0.29 (ΓA)	+0.104	KI, K(s)
Rb_2F		1+	1−	1+	7.85	31.6	84.9	3.00	0.64 (KΓ)	0.49 (ΓA)	+0.140	RbF, Rb(s)
Rb_2Cl		1+	1−	1+	8.63	32.0	87.1	2.52	0.61 (ΓM)		+0.076	RbCl, Rb(s)
Rb_2Br		1+	1−	1+	8.92	31.9	87.2	2.45	0.62 (ΓM)		+0.070	RbBr, Rb(s)
Rb_2I		1+	1−	1+	9.42	31.7	87.3	2.28	0.62 (ΓM)	0.45 (ΓA)	+0.077	RbI, Rb(s)
Cs_2F		1+	1−	1+	8.44	31.3	80.9	2.42	0.52 (KΓ)	0.41 (ΓA)	+0.121	CsF, Cs(s)
Cs_2Cl		1+	1−	1+	9.21	31.8	84.2	2.04	0.50 (ΓM)	0.23 (ΓA)	+0.054	CsCl, Cs(s)
Cs_2Br		1+	1−	1+	9.49	32.2	85.3	1.98	0.52 (ΓM)	0.42 (ΓA)	+0.045	CsBr, Cs(s)

[a]The definitions for the listed quantities are the same as those given in Table 1.

trigonal systems. Because we need empty layers for anionic electrons, the stacking pattern in the hexagonal symmetry should be of the $-A^cB^aA^c-e-B^cA^aB^c-e-A^cB^aA^c-$ or $-A^cB^aA^c-e-A^cB^aA^c-e-A^cB^aA^c-$ type, where −e− represent the empty layers for anionic electrons and the superscripts a and c indicate the anion and cation layers, respectively. In both cases, the types of cation layers in the ionic unit are the same (i.e., A-and-A in the $-A^cB^aA^c-$ unit and B-and-B in the $-B^cA^aB^c-$ unit), and the on-top stacking of the cation layers is highly unstable in energy. In fact, the former/latter type of artificial Ca_2N in the hexagonal symmetry shows higher energy by 0.67/0.71 eV per Ca_2N unit than the original Ca_2N in the trigonal symmetry. Therefore, the screening in the trigonal symmetry is a reasonable strategy.

We carried out high-throughput screening with the Materials Project for ternary electrides $A_nB_mC_k$, where element A is alkali or alkaline-earth metals. However, no candidates were found because the combinations of B and C elements always result in charge compensation, i.e., $[A_nB_mC_k]^{0\pm}$. The difficulty is partially related to the limited amount of compounds included in the database, and exploration using a larger database, such as the Inorganic Crystal Structure Database (ICSD),[27] may improve the results for ternary 2D electrides. However, charge compensation by elements B and C is expected for stable ternary materials, so that even exploration using a larger database may also fail. Therefore, we adopted another strategy in this study rather than a straightforward search based on a large database.

III-2. Screening-Driven Tailored Modeling with a New Indicator. *III-2a. Dialkali Halides as 2D Electrides.* The Ca_2N, Sr_2N, and Ba_2N 2D electrides are alkaline-earth nitrides; therefore, alkali halide electrides could also be a feasible target. To maintain the total charge condition, the formula unit of alkali halides for electrides must be A_2X because the formula leads to an anionic electron as $[A_2X]^+\cdot e^-$, where A is an alkali metal and X is a halogen. In addition, the trigonal structure is highly favorable for establishing 2D empty space, as with the nitride 2D electrides. However, stable alkali halides with the formula AX have cubic structures; therefore, the possibility of crystal structure transformation from cubic to trigonal should be discussed. This point will be investigated after discussion of the electronic structures of A_2X for 2D electrides.

Dialkali halides A_2X were computationally investigated using Li, Na, K, Rb, and Cs for A and F, Cl, Br, I for X. The layer structures of the compounds are easily constructed from the atomic positions of trigonal nitrides by substituting alkaline-earth metals with alkali metals and N with halogen. At first, structural relaxations to allow lattice deformation were performed using the trigonal lattice as the initial lattice. After full relaxation, the structures with all combinations of A and X, except for Cs_2I, maintained the trigonal lattice and empty 2D spaces. For Cs_2I, difficulty in convergence of the wave functions was encountered, and thus Cs_2I was not considered any further.

The relaxed lattice data, a_{ele}, bandwidths, and energy differences from the stable compounds are listed in Table 2. Of special note, almost all of the compounds listed in Table 2 have larger bandwidths (i.e., larger velocity of the anionic electrons) and larger a_{ele} than Ca_2N. In particular, the compounds Li_2F, Li_2Cl, Na_2F, and Na_2Cl, which consist of ubiquitous elements, exhibit quite large bandwidths. The band structure and partial electron density for Na_2Cl are shown in Figure 4.

In contrast to the dialkali halides with light alkali metals, some dialkali halides including heavy alkali metals have the band crossing on the ΓA line at the Fermi level, as listed in Table 2. The band dispersion along this line corresponds to dispersion along the z axis (i.e., [111] direction in Figure 1a,b), and therefore the confinement of electrons in 2D space at the Fermi level is partially broken. The energy band crossing the Fermi level on the ΓA line is not the band for the anionic electrons but the band for the alkali metals, which are already positioned at approximately 1 eV above the Fermi level in Na_2Cl (Figure 4). The bottom of the band shifts to the Fermi level for the heavy alkali metals. This trend can also be confirmed also in the three nitride 2D electrides; the positions

dx.doi.org/10.1021/ic501362b | Inorg. Chem. 2014, 53, 10347−10358

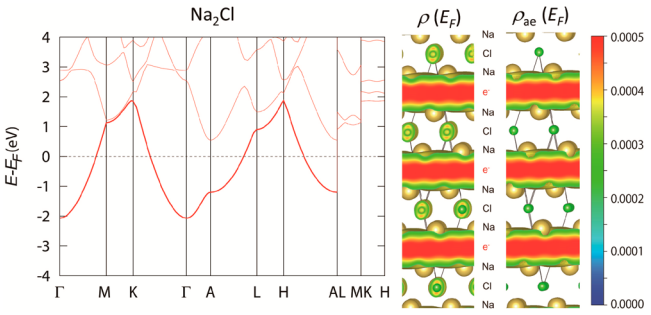

Figure 4. Calculated band structure and partial electron density for Na_2Cl. The red bold line in the band structure corresponds to the energy band for the anionic electrons. $\rho(E_F)$ is the partial electron density in the region from $E_F = -0.05$ to +0.05 eV, and $\rho_{ae}(E_F)$ is that of anionic electrons, which are depicted using the color scale (1/bohr^3).

of the band bottom on the ΓA line shift toward the Fermi level in the order of Ca_2N, Sr_2N, and Ba_2N (Figure 2).

The next concern is the stability of these compounds. All of the dialkali halides are unstable with respect to the existing reference compounds. Thus, a straightforward synthesis will fail for these dialkali halides. Therefore, we investigate the possibility of a synthesis that incorporates strain in the crystals. Bearing in mind the presence of the HPEs,[26] the synthesis using strain is rather a plausible way, although the stabilization mechanism of a HPE by hydrostatic pressure is different from that of a 2D electride by uniaxial or biaxial strain because the volume change expected in the hydrostatic pressure is not valid in the uniaxial or biaxial strain. The cubic structures of the stable AX compounds can be transformed to the trigonal form by crystal strain, as shown in Figure 5a. In addition to transformation of the crystal lattice, alkali metals have to be introduced in the strained AX structures. Thus, the energy difference to be investigated during the lattice deformation is $E^{diff} = E(A_2X) - [E(\text{strained AX}) + E(A(s))]$. During lattice deformation, the cubic lattice parameters, $[a(=b=c), 60°\ (=\alpha=\beta=\gamma)]$, change to trigonal lattice parameters, $[a'\ (=b'=c'), \alpha'\ (=\beta'=\gamma \neq 60°)]$, as listed in Table 2. In this study, we have assumed that the lattice size and angles are changed at equal rates; i.e., when the lattice size is extended by 10% of $(a' - a)$, the lattice angle is reduced by 10% of $(60 - \alpha')$. To define the strained structure, the lattice mismatch was introduced as $\{(a''/a) - 1\} \times 100$, where a'' is the lattice size during deformation, and thus a'' becomes a' when the cubic lattice is completely transformed to the trigonal structure.

Figure 5b shows the calculated energy differences as a function of the lattice mismatch for Li_2F and Na_2Cl. These two compounds were selected as systems to be strained because the energy differences of the compounds with respect to the stable alkali halides are relatively small at zero strain. The transition points (i.e., zero energy difference) for Li_2F and Na_2Cl are located at lattice mismatches of approximately 12.5 and 17.0%, respectively. Although the required lattice deformations are relatively large, the deformation energies of alkali metals, which are not included in the present calculations, will lead to a much easier transformation from the cubic to trigonal structure. The smaller strain required in Li_2F than in Na_2Cl is due to the larger Young's modulus of LiF than that of NaCl. A smaller energy difference at zero strain results in a smaller lattice deformation required for the cubic-to-trigonal transformation. As an example for Cs_2Br, the transformation can be easier at

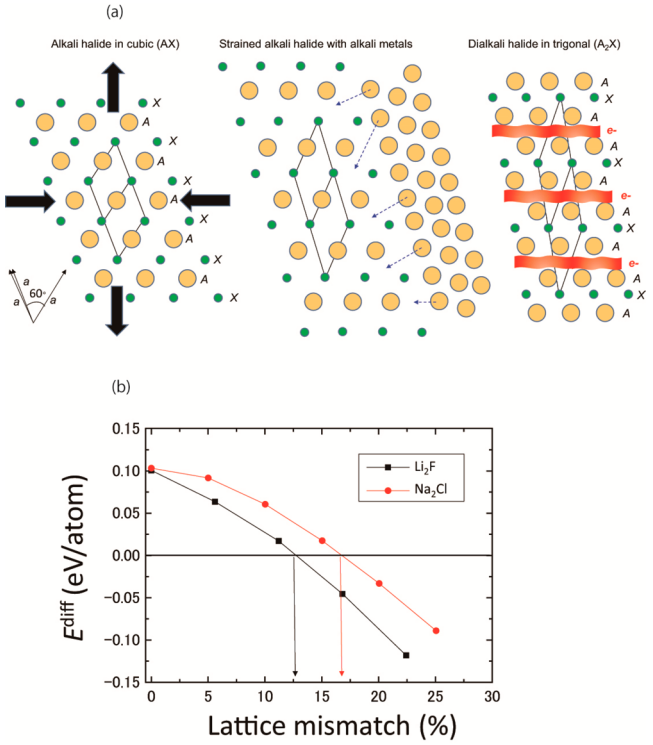

Figure 5. (a) Schematic diagram of the lattice deformation required for the cubic-to-trigonal transformation. (b) Calculated lattice mismatch required for the cubic-to-trigonal transformation in Li_2F and Na_2Cl.

approximately 8.5% of the required lattice mismatch (not shown), although Cs_2Br is not a suitable 2D electride compound because of the band crossing on the ΓA line.

III-2b. Ternary Oxides as 2D Electrides. In the previous sections, we have investigated nitrides and carbides from the Materials Project database, in addition to dialkali halides by screening-driven tailored modeling. In this section, the target compounds are oxides. In the ab initio screening with the Materials Project, trigonal Cs_2O remained before the final screening because Cs_2O has both a layered structure and empty 2D spaces; however, Cs_2O was filtered out at the final screening because the total formal charge is neutral. Cs_2O thus has a band gap, but the electrons at the bottom of the conduction band can be distributed in the empty 2D space. Thus, electron doping of Cs_2O would probably lead to a 2D electride (this point will be investigated in a later section on anion doping). Other dialkali oxides such as Na_2O, K_2O, and Rb_2O have cubic structures, and therefore 2D empty spaces between the ionic layers are not confirmed. However, electrons at the conduction band bottom in these compounds are localized at interstitial sites, as shown in Figure 6. Thus, if the cubic structures of such dialkali oxides can be changed to trigonal structures by chemical pressure (i.e., chemical doping), this series of oxides could also be candidates for 2D electrides.

The simplest way to introduce anionic electrons into the dialkali oxides A_2O is the exchange of an alkali metal with an alkaline-earth metal (Ae) to form AAeO, which can lead to an anionic electron, $[AAeO]^+ \cdot e^-$. Thus, a computational investigation was conducted using Na, K, and Rb for A and Be, Mg, Ca, Sr, and Ba for Ae. To check the structural stability of AAeO in the trigonal lattice, the structural relaxation of each AAeO compound was examined for both cubic and trigonal lattices.

dx.doi.org/10.1021/ic501362b | Inorg. Chem. 2014, 53, 10347−10358

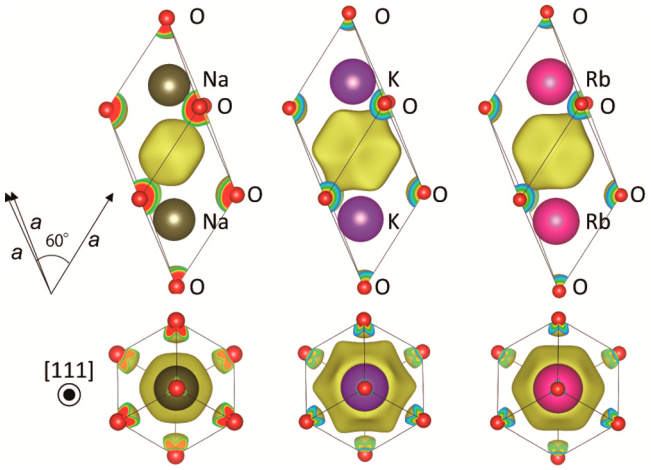

Figure 6. (a) Cubic structures of dialkali oxides Na_2O, K_2O, and Rb_2O along the [111] direction (top) and perpendicular to the [111] direction (bottom). The electrons at the conduction band bottom are depicted by yellow surfaces.

The relaxed trigonal AAeO compounds are interestingly more stable than the cubic lattice, which provides 2D empty spaces for the anionic electrons. In these calculations, the unit of ionic layers is designated as [AOAe]; i.e., alkali metals (or alkaline-earth metals) construct cation layers without a mixture of A and Ae. This assumption seems to be somewhat artificial, but it was confirmed that a separated layer structure in KCaO, such as K(B)O(A)Ca(C)−K(A)O(C)Ca(B)−K(C)O(B)Ca(A)−K-(B)O(A)Ca(C) (note the expression for the layer indices in Figure 1), makes the system more stable than a K-and-Ca mixed layer system. It was also confirmed that when the level of mixture becomes high, the destabilization energy from the unmixed (i.e., separated) structure is increased. Thus, the computational models for the ternary systems adopted in this study support the complete separation of alkali and alkaline-earth metals in all cationic layers.

The relaxed lattice data, a_{ele}, bandwidths, and energy differences from the stable compounds are listed in Table 3. As with the dialkali halide A_2X compounds, almost all of the AAeO compounds listed in Table 3 have larger bandwidths and larger a_{ele} than Ca_2N. In particular, the NaMgO, KMgO, and RbMgO compounds have very large bandwidths. However, in contrast to the dialkali halides, the destabilization energy of AAeO is very large with respect to the stable oxides because of the higher stability of the reference oxides. However, if AAeO compounds could be synthesized from the cubic A_2O, alkali, and alkaline-earth metals, the relative energies of AAeO compounds, except for KBeO and RbBeO, become negative, which indicates the possibility of AAeO synthesis by avoiding the oxidation process of the alkaline-earth metals. The band

Table 3. Relaxed Lattice Data, Calculated Properties for Anionic Electrons, and Energetic Stabilities for the Alkaline-Earth-Doped Alkali Oxides (AAeO) Identified by Screening-Driven Tailored Modeling[a]

ABC	ID	VA	VB	VC	FC	a (Å)	α (deg)	a_{ele} (%)	W_{ae} (eV)	v_{2Dmax} ($\times 10^8$ cm/s)	v_{zmax} ($\times 10^8$ cm/s)	E^{diff} (eV/atom)	C^{ref}
NaBeO		1+	2+	2−	1+	7.37	21.9	82.4	6.76	1.06 (ΓM)	0.80 (ΓA)	+0.396	BeO, Na(s)
												−0.230	Na_2O, Na(s), Be(s)
NaMgO		1+	2+	2−	1+	6.00	31.0	82.6	5.60	0.92 (KΓ)		+0.311	MgO, Na(s)
												−0.281	Na_2O, Na(s), Mg(s)
NaCaO		1+	2+	2−	1+	6.40	32.1	84.5	3.65	0.70 (KΓ)		+0.307	CaO, Na(s)
												−0.453	Na_2O, Na(s), Ca(s)
NaSrO		1+	2+	2−	1+	6.74	32.3	85.3	3.44	0.67 (KΓ)		+0.272	SrO, Na(s)
												−0.335	Na_2O, Na(s), Sr(s)
NaBaO		1+	2+	2−	1+	7.04	32.8	83.5	3.03	0.60 (KΓ)		+0.213	BaO, Na(s)
												−0.220	Na_2O, Na(s), Ba(s)
KBeO		1+	2+	2−	1+	6.18	27.3	70.2	3.83	0.50 (KΓ)	0.18 (LM)	+0.899	BeO, K(s)
												+0.083	K_2O, K(s), Be(s)
KMgO		1+	2+	2−	1+	6.62	29.2	79.7	4.38	0.69 (KΓ)		+0.477	MgO, K(s)
												−0.305	K_2O, K(s), Mg(s)
KCaO		1+	2+	2−	1+	7.14	29.7	83.7	3.22	0.62 (ΓM)		+0.370	CaO, K(s)
												−0.581	K_2O, K(s), Ca(s)
KSrO		1+	2+	2−	1+	7.40	30.3	85.0	3.09	0.60 (ΓM)		+0.282	SrO, K(s)
												−0.515	K_2O, K(s), Sr(s)
KBaO		1+	2+	2−	1+	7.69	30.8	83.8	2.76	0.54 (KΓ)		+0.181	BaO, K(s)
												−0.443	K_2O, K(s), Ba(s)
RbBeO		1+	2+	2−	1+	6.22	28.2	55.0		0.97 (KΓ)	0.60 (ΓA)	+1.097	BeO, Rb(s)
												+0.165	Rb_2O, Rb(s), Be(s)
RbMgO		1+	2+	2−	1+	6.89	28.5	77.8	4.05	0.62 (KΓ)		+0.584	MgO, Rb(s)
												−0.314	Rb_2O, Rb(s), Mg(s)
RbCaO		1+	2+	2−	1+	7.41	29.1	82.5	3.14	0.58 (KΓ)		+0.431	CaO, Rb(s)
												−0.635	Rb_2O, Rb(s), Ca(s)
RbSrO		1+	2+	2−	1+	7.70	29.5	83.9	3.02	0.58 (KΓ)	0.31 (ΓA)	+0.321	SrO, Rb(s)
												−0.592	Rb_2O, Rb(s), Sr(s)
RbBaO		1+	2+	2−	1+	7.95	30.2	82.7	2.74	0.54 (KΓ)		+0.201	BaO, Rb(s)
												−0.538	Rb_2O, Rb(s), Ba(s)

[a]The definitions for the listed quantities are the same as those given in Table 1.

dx.doi.org/10.1021/ic501362b | Inorg. Chem. 2014, 53, 10347−10358

structure and partial electron density for NaMgO are shown in Figure 7.

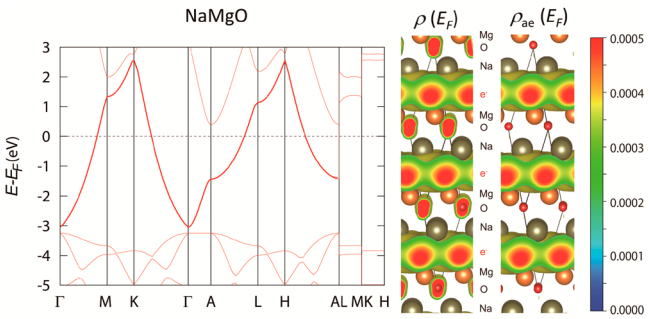

Figure 7. Calculated band structure and partial electron density for NaMgO. The red bold line in the band structure corresponds to the energy band for the anionic electrons. $\rho(E_F)$ is the partial electron density in the region from $E_F = -0.05$ to +0.05 eV, and $\rho_{ae}(E_F)$ is that of anionic electrons, which are depicted using the color scale (1/bohr^3).

III-2c. Ternary Carbides as 2D Electrides. In section III-1b on Y_2C, we stated that Y_2C has two anionic electrons per unit, which causes an increase in the Fermi level and thereby the partial capture of electrons by the d orbitals of Y. When a single Y atom per unit is exchanged with an alkaline-earth metal Ae, a single anionic electron per formula unit is introduced as $[YAeC]^+\cdot e^-$, and the confinement of anionic electrons in the 2D empty spaces is expected.

Alkaline-earth-doped Y_2C (i.e., YAeC) compounds were computationally investigated using Be, Mg, Ca, Sr, and Ba for Ae. After structural relaxation, it was confirmed that all of the compounds in this series take stable atomic positions in the trigonal lattice. However, YBeC does not have anionic electrons in the 2D empty spaces between ionic layers because the electrons at the Fermi level are mainly projected onto the d orbitals of Y, and a_{ele} for YBeC is 0.4%. The lattice parameter for YBeC is significantly reduced to 4.51 Å, so that the system cannot maintain the 2D empty spaces.

Table 4 lists the relaxed lattice data, a_{ele}, bandwidths, and energy differences for the stable YMgC, YCaC, YSrC, and YBaC materials. The DOSs at the Fermi level are difficult to project onto atomic orbitals of the constituent elements, and thus a_{ele} values are improved especially for YCaC, YSrC, and YBaC. However, the stabilities of these compounds with respect to the stable compounds are very poor.

III-2d. Oxides and Carbides as Ternary 2D Electrides by Anion Doping. The compounds investigated in the previous sections can be regarded as ternary systems obtained by the cation doping/substitution of binary systems to design the appropriate formal charge states for electrides, $[A_nB_mC_k]^+\cdot e^-$, where elements A and B are cations and C is an anion. In this section, we investigate ternary 2D electrides formed by anion doping. The target compounds are $[A_nC_mD_k]^+\cdot e^-$, where elements C and D are anions. Cs_2O and Y_2C were adopted here as the base binary compounds for anion doping/substitution.

Figure 8a shows the calculated band structure and partial electron density at the bottom of the conduction band for

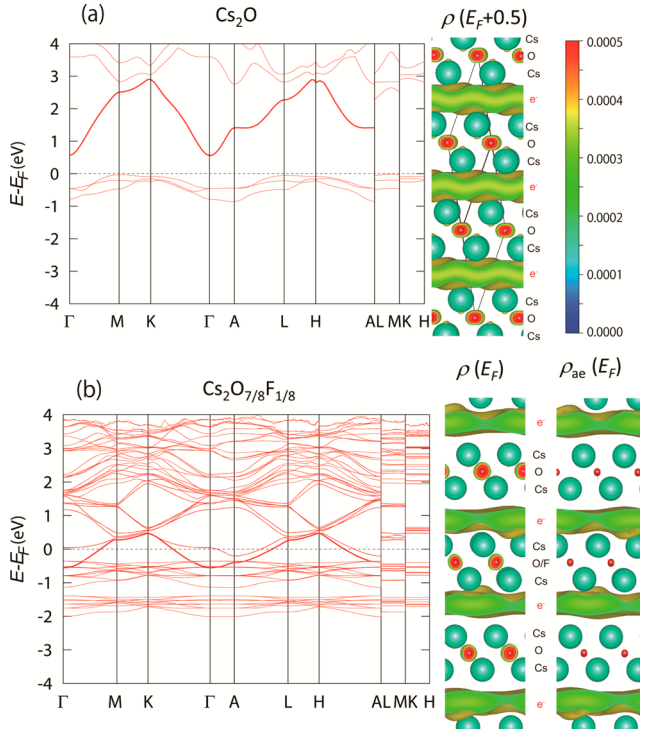

Figure 8. Calculated band structures and partial electron densities for (a) Cs_2O and (b) $Cs_2O_{1-x}F_x$ with $x = {}^1/_8$. The red bold line in the band structure corresponds to the energy band for the anionic electrons. $\rho(E_F)$ is the partial electron density integrated in the energy region from $E_F = -0.05$ to +0.05 eV, and $\rho_{ae}(E_F)$ is that of the anionic electrons, which are depicted using the color scale (1/bohr^3).

Cs_2O. The electrons at the bottom of the conduction band are confined between the Cs_2O neutral layers, and thus halogen-doped Cs_2O is a suitable ternary system (i.e., $[Cs_2O_{1-a}X_a]^{+a}\cdot ae^-$, where X is a halogen) to shift the Fermi level up to the bottom of the conduction band. Halogen-doped Cs_2O compounds were calculated using F, Cl, and Br for X. Figure

Table 4. Relaxed Lattice Data, Calculated Properties for Anionic Electrons, and Energetic Stabilities for the Alkaline-Earth-Doped Yttrium Carbides (YAeC) Identified by Screening-Driven Tailored Modeling[a]

ABC	ID	VA	VB	VC	FC	a (Å)	α (deg)	a_{ele} (%)	W_{ae} (eV)	v_{2Dmax} (×10^8 cm/s)	v_{zmax} (×10^8 cm/s)	E^{diff} (eV/atom)	C^{ref}
Y_2C	1334	3+		4−	2+	6.47	32.4	27.4	1.63	0.34 (MK)			
YBeC		3+	2+	4−	1+	4.51	44.1	0.4		0.32 (ΓM)	0.52 (ΓA)	+0.221	Y_2C, Y(s), Be(s)
YMgC		3+	2+	4−	1+	5.74	36.5	24.3	2.17	0.29 (ΓM)	0.36 (ΓA)	+0.367	Y_2C, Y(s), Mg(s)
YCaC		3+	2+	4−	1+	6.74	31.9	47.5	1.58	0.33 (ΓM)		+0.263	Y_2C, Y(s), Ca(s)
YSrC		3+	2+	4−	1+	7.04	31.3	52.6	1.60	0.34 (KΓ)		+0.376	Y_2C, Y(s), Sr(s)
YBaC		3+	2+	4−	1+	7.36	30.2	44.5	1.89	0.37 (MK)		+0.460	Y_2C, Y(s), Ba(s)

[a]The definitions for the listed quantities are the same as those given in Table 1.

dx.doi.org/10.1021/ic501362b | Inorg. Chem. 2014, 53, 10347−10358

Table 5. Relaxed Lattice Data, Calculated Properties for Anionic Electrons, and Energetic Stabilities for the Halogen-Doped Alkali Oxides and Hydrated Diyttrium Carbides Identified by Screening-Driven Tailored Modeling[a]

ABC	ID	VA	VB	VC	FC	a (Å)	α (deg)	a_{ele} (%)	W_{ae} (eV)	v_{2Dmax} ($\times 10^8$ cm/s)	v_{zmax} ($\times 10^8$ cm/s)	E^{diff} (eV/atom)	C^{ref}
Cs_2O	7988	1+	2−		0	7.76	31.9						
$Cs_2O_{7/8}F_{1/8}$		1+	2−	1−	1/8+	8.63	28.9	76.5	1.03	0.42 (KΓ)		−0.222	Cs_2O, F(g)
												−0.001	Cs_2O, CsF
$Cs_2O_{7/8}Cl_{1/8}$		1+	2−	1−	1/8+	8.37	30.4	74.5	1.01	0.42 (KΓ)	0.17 (ΓA)	−0.167	Cs_2O, Cl(g)
												+0.022	Cs_2O, CsCl
$Cs_2O_{7/8}Br_{1/8}$		1+	2−	1−	1/8+	8.35	30.8	74.4	1.02	0.43 (KΓ)	0.18 (ΓA)	−0.119	Cs_2O, Br(g)
												+0.032	Cs_2O, CsBr
Y_2C	1334	3+	4−		2+	6.47	32.4	27.4	1.63	0.34 (MK)			
Y_2CH (a)		3+	4−	1−	1+	6.11	34.4	0.07				−0.255	Y_2C, H(g)
Y_2CH (b)		3+	4−	1−	1+	6.20	35.0	14.9				−0.043	Y_2C, H(g)
$Y_2CH_{1/8}$		3+	4−	1−	15/8+	6.43	32.6	27.0				−0.042	Y_2C, H(g)

[a]The definitions for the listed quantities are the same as those given in Table 1.

8b shows the calculated band structure and partial electron density at the Fermi level for $Cs_2O_{1-x}F_x$, $x = {}^1/_8$. The optimized structure still maintains the layered structure, and the electrons at the Fermi level are confined between the $Cs_2O_{1-x}F_x$ layers. a_{ele} is calculated to be 76.5% and v_{2Dmax} is 0.42×10^8 cm/s on the KΓ line.[28] Therefore, $Cs_2O_{1-x}F_x$ ($x = {}^1/_8$) could be a good candidate for a ternary 2D electride. In addition, the relative energies of $Cs_2O_{1-x}F_x$ ($x = {}^1/_8$) with respect to the reference compounds (Cs_2O, CsF) and (Cs_2O, Cs(s), F(g)) are respectively −0.0007 and −0.2216 eV/atom, which indicates the possibility of F doping in the Cs_2O system. The same calculations were executed for other halogen-doped systems; however, the energy bands on the ΓA line slightly cross the Fermi level, and thus the doping of Cs_2O with other halogens is not very suitable for 2D electrides. The calculated results for the halogen-doped Cs_2O systems are listed in Table 5.

For anion doping of Y_2C, hydration of Y_2C is investigated; the formula is $[Y_2CH]^+ \cdot e^-$, where the H atom is not H^+ but H^- because one of two anionic electrons per Y_2C unit will be trapped by the H atom. This material is an analogue of Ca_2InN, which is a recently reported superconductor.[29] The doped H atom was positioned in the 2D empty space as an initial position, and the Y_2CH structure was fully relaxed. The electronic structure of the relaxed Y_2CH, which has the trigonal lattice, has a deep level localized around the doped H atom, and thus the H atom can be recognized as H^-. However, the band for anionic electrons completely disappears by the doping, and thereby a_{ele} is significantly decreased to 0.07%. The disappearance of the anionic electron band is probably related to the position of the H atom (2D empty space). Thus, another configuration with the H atom positioned at the centroid of a triangle consisting of three Y atoms was also fully relaxed, by which a_{ele} was increased to 14.9%. However, the structure is less stable than that with a H atom in the 2D empty space. Besides, the improved a_{ele} (14.9%) is still not as attractive as the original (i.e., a_{ele} of 27.4% for Y_2C). Doping with a small amount of H was also investigated to avoid destruction of the anionic electron band; however, the anionic electron band could still not be obtained around the Fermi level. The electrons are rather localized at interstitial sites to avoid the doped H atom, although localization, consequently, improves the number ratio a_{ele} to 27.0% but is still smaller than the original a_{ele}. Therefore, anionic doping of Y_2C using the H atom is not effective for improving the properties for 2D electrides.

III-3. Where Are the Next 2D Electrides? We investigated candidate compounds for 2D electrides using the Materials Project database and screening-driven tailored modeling. A total of 49 compounds were characterized in terms of their structures, number ratios of anionic electrons, bandwidths, maximum velocity of anionic electrons, and energy differences from stable compounds. Let us finally consider the critical directions for the next 2D electrides based on the calculated data.

In this study, we introduced the number ratio of anionic electrons at the Fermi level. The number ratios have an approximately monotonic relationship with the calculated bandwidths of the anionic electrons, as shown in Figure 9a. The bandwidths are almost proportional to the maximum velocities of anionic electrons (not shown); therefore, the number ratio a_{ele} or bandwidths W_{ae} of anionic electrons can be a good measure for the electronic conductive performance as 2D electrides. Note that in Figure 9 the samples showing band dispersions along ΓA, LM, or KH lines (e.g., NaBeO in Table 3) are excluded because these samples cannot be recognized as 2D electrides. In addition, the anion-doped cases (Table 5) are also excluded from this plot.

As shown in Figure 9a, the bandwidths are more suitable for determining the critical factors for 2D electrides than the number ratios of anionic electrons because the number ratios are rather concentrated in the two regions. Therefore, the binary and ternary compounds were first characterized using the bandwidths of anionic electrons. We also introduce the ratio of ionic radii, which is simply defined as $R^{ion} = r_c/r_a$, where r_c and r_a is are Pauling's ionic radius for the cation and anion, respectively. For the ternary compounds that include two different cations, r_c is defined as the average of the two ionic radii. Figure 9b shows the bandwidths of the anionic electrons W_{ae}, as a function of the ionic ratios. The samples shown can be divided into two regions, $R^{ion} > 0.8$ and $R^{ion} < 0.8$. In the region where $R^{ion} > 0.8$, the bandwidths are approximately 3 eV and not so sensitive to the ionic ratios. This region can be interpreted as $R^{ion} = 0.9 \pm 0.1$, and therefore the insensitive bandwidths are probably a result of the balanced ionic ratio. In contrast, the region where $R^{ion} < 0.8$ (i.e., unbalanced region) has bandwidths that are widely distributed from 1.5 to 5.7 eV. Three distinct categories are evident: (i) high band dispersions in Li_2F, Na_2F, and NaMgO; (ii) moderate band dispersions in the other dialkali halides, oxides, and nitrides; (iii) low band dispersions in the carbides. In addition, for each type of Ae_2N,

dx.doi.org/10.1021/ic501362b | Inorg. Chem. 2014, 53, 10347−10358

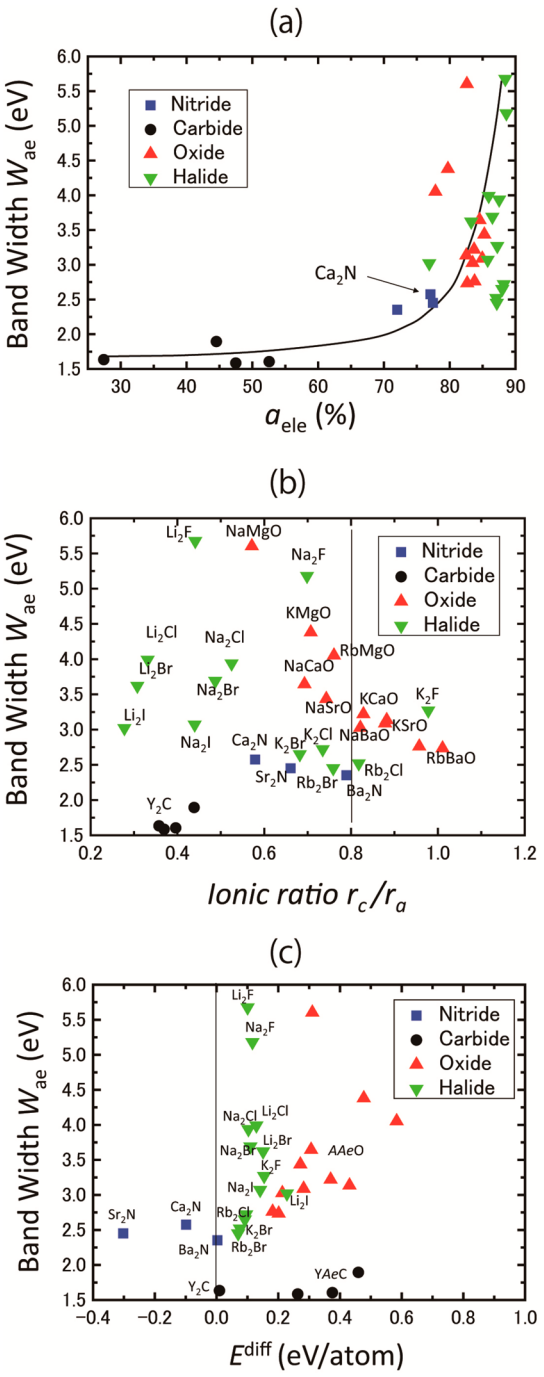

Figure 9. Calculated bandwidths W_{ae} for anionic electrons in nitrides, carbides, oxides, and halides as a function of (a) the number ratio of anionic electrons, a_{ele}, (b) the ionic ratio based on Pauling's ionic radii, and (c) the energy difference with respect to the reference compounds listed in Tables 1−4

A_2X, and AAeO compound, the heavier elements lead to smaller bandwidths of anionic electrons; for example, (i) 2.57 eV (Ca_2N), 2.45 eV (Sr_2N), 2.35 eV (Ba_2N), (ii) 5.67 eV (Li_2F), 3.99 eV (Li_2Cl), 3.62 eV (Li_2Br), 3.02 eV (Li_2I), (iii) 5.67 eV (Li_2F), 5.18 eV (Na_2F), 3.27 eV (K_2F), 3.00 eV (Rb_2F), and (iv) 6.76 eV (NaBeO), 5.60 eV (NaMgO), 3.65 eV (NaCaO), 3.44 eV (NaSrO), and 3.03 eV (NaBaO). This is probably due to enlargement of the lattice size by the heavier elements because the transfer integral of anionic electrons decreases with increasing lattice size, which results in smaller bandwidths. Therefore, light elements are preferable for designing a large band dispersion (i.e., larger velocity of anionic electrons) in 2D electrides. In consideration of this concept, better electronic properties are expected for Mg_2N than for Ca_2N. Fully relaxed Mg_2N with a trigonal lattice exhibits better properties for 2D electrides such as W_{ae} of 3.9 eV, v_{2Dmax} of 1.01×10^8 cm/s, and no bands crossing the Fermi level on the ΓA, LM, and KH lines, although a_{ele} is slightly smaller than that for the other nitrides; a_{ele} calculated for Mg_2N is 62.1%. However, the stability of Mg_2N with respect to the existing compounds is quite poor; the energy difference from Mg_3N_2 is calculated to be +0.18 eV/atom. The instability is almost comparable to the AAeO oxide series. Consequently, Mg_2N cannot be a new target 2D electride.

Finally, the relationship between the bandwidths of anionic electrons W_{ae} and the energy differences E^{diff} with respect to stable compounds was analyzed, as shown in Figure 9c. The stable compounds used in the calculations for the energy differences are listed in Tables 1−5 as C^{ref}, and this corresponds to an extremely dilute gas condition. In the characterization, the data by lattice deformation in the dialkali halides A_2X and those to avoid the oxidation of alkali metals in AAeO are excluded for simplicity. The results indicate that all of the compounds, except for the three nitrides (Ca_2N, Sr_2N, and Ba_2N) and Y_2C, are relatively difficult to synthesize from stable compounds. The AAeO oxides are particularly difficult to synthesize because of the high stability of the alkaline-earth oxides; the energy differences from stable compounds are at least +0.2 eV/atom. Thus, if the oxidation process of alkaline-earth metals can be avoided during the synthesis of AAeO, then the energy differences from the basic compounds of A_2O, A, and Ae change significantly to large negative values (Table 3). In contrast to the oxides, the energy differences of the dialkali halides are at most +0.2 eV/atom, which indicates the relative ease of synthesis compared with the oxides. For example, the minimum energy difference for Rb_2Br is +0.07 eV/atom. In the group of dialkali halides, the bandwidths are spread widely from 2 to 6 eV, which provides the possibility to obtain new 2D electrides with larger Fermi velocities of anionic electrons than that of Ca_2N. This figure also shows that there is an open space at the left upper area, i.e., the area of large band dispersions and high stabilities. Although no compounds were found in the area, the present high-throughput screening does find the existence of an attractive area for high-performance 2D electrides to be explored extensively.

IV. SUMMARY AND CONCLUSIONS

High-throughput ab initio screening was conducted to identify binary and ternary 2D electrides using a high-throughput ab initio screening platform, the Materials Project. Exploration based on the Materials Project database utilized three indicators: (1) a positive formal charge per unit formula; (2) layered structures for two-dimensionality; (3) 2D empty spaces for anionic electrons. Three binary nitrides, Ca_2N, Sr_2N, and Ba_2N, and a carbide, Y_2C, were determined as candidates. The number ratio of anionic electrons at the Fermi level a_{ele} was introduced to characterize the 2D electrides explicitly. The three nitrides show large a_{ele} (70−80%), whereas that for Y_2C was a smaller value of a_{ele} (27%) because of the partial occupation of anionic electrons in the d orbitals of Y. These results, together with the lack of candidates from the p-block elements, led to the design of 2D electrides including s-group

dx.doi.org/10.1021/ic501362b | Inorg. Chem. 2014, 53, 10347−10358

elements (i.e., alkali or alkaline-earth metals). Ab initio calculations based on the design found the following:

(1) The Fermi velocities of anionic electrons in the dialkali halides (A_2X) and alkaline-earth-doped alkali oxides (AAeO) can be larger than that of Ca_2N, but the relative energetic instabilities of A_2X and AAeO with respect to the stable compounds indicate the difficulty of straightforward synthesis; therefore, from a theoretical basis, possible synthetic routes are proposed by the introduction of strain for A_2X and by avoiding oxidation of alkaline-earth metals during the synthesis of AAeO.

(2) Alkaline-earth-doped yttrium carbides (YAeC) do not exhibit better properties as 2D electrides than those of Ca_2N, and the syntheses of YAeC are quite difficult.

(3) The Fermi velocity of anionic electrons in F-doped Cs_2O ($Cs_2O_{1-x}F_x$ with $x = {}^1/_8$) is comparable with that in Ca_2N, and the relative energetic stability in F-doped Cs_2O indicates the high possibility for the synthesis of the oxide 2D electride.

To determine the critical directions for the next-generation 2D electrides, the calculated data were analyzed using the ionic ratio R^{ion}, which is defined as the ratio of the cation ionic radius to that of the anion, bandwidths of anionic electrons W_{ae}, and the energy differences from stable compounds E^{diff}, and found the following:

(4) The calculated compounds are categorized into two regions: the balanced region ($0.8 < R^{ion} < 1.0$), where W_{ae} is approximately 3 eV, and the unbalanced region ($0.8 > R^{ion}$), where the bandwidths are widely distributed from 1.5 to 5.7 eV. The three nitrides and dialkali halides except for K_2F are unbalanced compounds, whereas the alkaline-earth-doped alkali oxides (AAeO) are positioned around the boundary of $R^{ion} = 0.8$.

(5) The W_{ae} versus R^{ion} plot revealed that four dialkali halides, K_2Cl, K_2Br, Rb_2Cl, and Rb_2Br, are positioned very closely to the three nitrides, and E^{diff} for the dialkali halides from the stable compounds are relatively small; E^{diff} for K_2Cl, K_2Br, Rb_2Cl, and Rb_2Br are +0.095, +0.092, +0.076, and +0.070 eV/atom, respectively.

Thus, one new 2D electride can be expected from the four dialkali halides. In addition, if E^{diff} of ca. 0.1 eV/atom is acceptable, then we can focus our attention on another group of dialkali halides, such as Li_2F and Na_2Cl, which have very large band dispersions of anionic electrons. This provides an attractive and challenging direction. Of course, Sr_2N, Ba_2N, Y_2C, and F-doped Cs_2O are highly promising candidates because of their relative energetic stabilities with respect to the stable compounds.

■ ASSOCIATED CONTENT

Supporting Information

Pauling and Shannon ionic radii used for calculation of the number ratio of anionic electrons, the calculated number ratios of anionic electrons, and a correlation map of these ratios. This material is available free of charge via the Internet at http://pubs.acs.org.

■ AUTHOR INFORMATION

Corresponding Author

*E-mail: tada.t.ae@m.titech.ac.jp.

Notes

The authors declare no competing financial interest.

■ ACKNOWLEDGMENTS

This study was supported by the "Element strategy Initiative to Form Core Research Center" of the Ministry of Education, Culture, Sports, Science and Technology of Japan and by the Japan Science and Technology Agency ACCEL program.

■ REFERENCES

(1) Ellaboudy, A.; Dye, J. L.; Smith, P. B. *J. Am. Chem. Soc.* **1983**, *105*, 6490−6491.

(2) Matsuishi, S.; Toda, Y.; Miyakawa, M.; Hayashi, K.; Kamiya, T.; Hirano, M.; Tanaka, I.; Hosono, H. *Science* **2003**, *301*, 626−629.

(3) Kitano, M.; Inoue, Y.; Yamazaki, Y.; Hayashi, F.; Kanbara, S.; Matsuishi, S.; Yokoyama, T.; Kim, S.-W.; Hara, M.; Hosono, H. *Nat. Chem.* **2012**, *4*, 934−940.

(4) Takahashi, H.; Igawa, K.; Arii, K.; Kamihara, Y.; Hirano, M.; Hosono, H. *Nature* **2008**, *453*, 376−378.

(5) Li, L.; Richter, C.; Mannhart, J.; Ashoori, R. C. *Nat. Phys.* **2011**, *7*, 762−766.

(6) Lee, K.; Kim, S.-W.; Toda, Y.; Matsuishi, S.; Hosono, H. *Nature* **2013**, *494*, 336−341.

(7) Curtarolo, S.; Hart, G. L. W.; Nardelli, M. B.; Mingo, N.; Sanvito, S.; Levy, O. *Nat. Mater.* **2013**, *12*, 191−201.

(8) Hautier, G.; Miglio, A.; Ceder, G.; Rignanese, G.-M.; Gonze, X. *Nat. Commun.* **2013**, *4*, 1−7.

(9) Curtarolo, S.; Setyawan, W.; Hart, G. L. W.; Jahnatek, M.; Chepulskii, R. V.; et al. *Comput. Mater. Sci.* **2012**, *58*, 218−226.

(10) Jain, A.; Hautier, G.; Moore, C. J.; Ong, S. P.; Fischer, C. C.; Mueller, T.; Persson, K. A.; Ceder, G. *Comput. Mater. Sci.* **2011**, *50*, 2295−2310.

(11) Curtarolo, S.; Setyawan, W.; Wang, S.; Xue, J.; Yang, K.; Taylor, R. H.; Nelson, L. J.; Hart, G. L. W.; Sanvito, S.; Buongiorno-Nardelli, M.; Mingo, N.; Levy, O. *Comput. Mater. Sci.* **2012**, *58*, 227−235.

(12) Ceder, G. *Mater. Res. Soc. Bull.* **2010**, *35*, 693−701.

(13) Jain, A.; Ong, S. P.; Hautier, G.; Chen, W.; Richards, W. D.; Dacek, S.; Cholia, S.; Gunter, D.; Skinner, D.; Ceder, G.; Persson, K. A. *Appl. Phys. Lett. Mater.* **2013**, *1*, 011002.

(14) Ong, S. P.; Richards, W. D.; Jain, A.; Hautier, G.; Kocher, M.; Cholia, S.; Gunter, D.; Chevrier, V. L.; Persson, K. A.; Ceder, G. *Comput. Mater. Sci.* **2013**, *68*, 314−319.

(15) Yu, L.; Zunger, A. *Phys. Rev. Lett.* **2012**, *108*, 068701.

(16) Kresse, G.; Furthmüller, J. *Comput. Mater. Sci.* **1996**, *6*, 15−50.

(17) Blöchl, P. *Phys. Rev. B* **1994**, *50*, 17953−17979.

(18) Perdew, J.; Burke, K.; Ernzerhof, M. *Phys. Rev. Lett.* **1996**, *77*, 3865−3868.

(19) The energy cutoff is set to be 1.3 times larger than that specified in the pseudopotential. A total of $1000/n$ *points* are used as k points, where n is the number of atoms in the unit cell. The thresholds for electronic energy convergence and ionic convergence are $n \times 5 \times 10^{-5}$ and $n \times 5 \times 10^{-4}$ eV, respectively.

(20) http://jp-minerals.org/vesta/jp/.

(21) Inoshita, T.; Jeong, S.; Hamada, N.; Hosono, H. *Phys. Rev. X* **2014**, *4*, 031023.

(22) Walsh, A.; Scanlon, D. O. *J. Mater. Chem. C* **2013**, *1*, 3525−3528.

(23) Pauling, L. *The Nature of the Chemical Bond*, 3rd ed.; Cornell University Press: Ithaca, NY, 1960.

(24) Shannon, R. D.; Prewitt, C. T. *Acta Crystallogr.* **1969**, *B25*, 925−945.

(25) Shannon, R. D. *Acta Crystallogr.* **1976**, *A32*, 751−767.

(26) Miao, M.-S.; Hoffmann, R. *Acc. Chem. Res.* **2014**, *47*, 1311−1317.

(27) http://www.fiz-karlsruhe.de/icsd.html?&L=0.

(28) The bandwidth of $Cs2O_{1-x}F_x$ is 2 times smaller than that of Ca_2N, but the velocity is comparable to that of Ca_2N because the lattice size of $Cs_2O_{1-x}F_x$ is about 2 times larger than that of Ca_2N to realize the F doping with the amount of $x = {}^1/_8$ (i.e., the unit cell includes $Cs_{16}O_7F_1$).

(29) Jeong, S.; Matsuishi, S.; Lee, K.; Toda, Y.; Kim, S.-W.; Hosono, H. *Supercond. Sci. Technol.* **2014**, *27*, 055005.